Downregulation of Tomato *STEROL GLYCOSYLTRANSFERASE 1* Perturbs Plant Development and Facilitates Viroid Infection

Adriana E. Cisneros[a], Purificación Lisón[a], Laura Campos[a], Joan Manel López-Tubau[b], Teresa Altabella[b,c], Albert Ferrer[b,d], José-Antonio Daròs[a], Alberto Carbonell[a,*]

[a]*Instituto de Biología Molecular y Celular de Plantas (Consejo Superior de Investigaciones Científicas–Universitat Politècnica de València), 46022 Valencia, Spain*

[b]*Centre for Research in Agricultural Genomics (CSIC-IRTA-IAB-UB), Bellaterra, Barcelona, Spain*

[c]*Department of Biology, Healthcare and the Environment, Faculty of Pharmacy and Food Sciences, University of Barcelona, 08028 Barcelona, Spain*

[d]*Department of Biochemistry and Physiology, Faculty of Pharmacy and Food Sciences, University of Barcelona, 08028 Barcelona, Spain*

*Corresponding author

Author's e-mail addresses:

Adriana E. Cisneros: adgoncis@ibmcp.upv.es

Purificación Lisón: plison@ibmcp.upv.es

Laura Campos: laucambe@upvnet.upv.es

Joan Manel López-Tubau: joanmanel.lopez@cragenomica.es

Teresa Altabella: taltabella@ub.edu

Albert Ferrer: albertferrer@ub.edu

José-Antonio Daròs: jadaros@ibmcp.upv.es

Alberto Carbonell: acarbonell@ibmcp.upv.es

HIGHLIGHT

Depletion of glycosylated sterols in tomato plants induces developmental and reproductive defects such as leaf epinasty, dwarfism and reduced fruit size, as well as hypersusceptibility to viroid infection.

ABSTRACT

Potato spindle tuber viroid (PSTVd) is a plant pathogen naturally infecting economically important crops such as tomato (*Solanum lycopersicum*). Here, we aimed to engineer tomato plants highly resistant to PSTVd and developed several *S. lycopersicum* lines expressing an artificial microRNA (amiRNA) against PSTVd (amiR-PSTVd). Infectivity assays revealed that amiR-PSTVd-expressing lines were not resistant but rather hypersusceptible to the viroid. A combination of phenotypic, molecular and metabolic analyses of amiRNA-expressing lines non-inoculated with the viroid revealed that amiR-PSTVd was accidentally silencing the tomato *STEROL GLYCOSYLTRANSFERASE 1* (*SlSGT1*) gene, which caused late developmental and reproductive defects such as leaf epinasty, dwarfism or reduced fruit size. Importantly, two independent transgenic tomato lines each expressing a different amiRNA specifically designed to target *SlSGT1* were also hypersusceptible to PSTVd, thus confirming that downregulation of *SlSGT1* was responsible for the viroid hypersusceptibility phenotype. Our results highlight the role of SGTs in proper plant development and indicate that the unbalance of sterol glycosylation levels favors viroid infection most likely by facilitating viroid movement.

Keywords: artificial microRNA, sterol glycosyltransferase, viroid, hypersusceptibility, *Solanum lycopersicum*

INTRODUCTION

Viroids are plant pathogens composed of a small [250-400 nucleotides (nts)], circular, single-stranded RNA genome without protein-coding capacity (Navarro et al., 2021a). They induce symptoms in infected plants such as stunting, chlorosis, leaf curling, bark alterations, and size reduction of fruits and tubers (Flores et al., 2005). Viroids replicate through an RNA-based rolling-circle mechanism (Branch and Robertson, 1984), move cell to cell via plasmodesmata and long-distance through the phloem stream (Pallás and Gómez, 2017), and are classified into the *Pospiviroidae* or *Avsunviroidae* families whose members replicate and accumulate in the nucleus and chloroplasts, respectively (Flores et al., 2015; Daros, 2016). Viroid pathogenesis is a complex process regulated by multiple factors including i) the alteration of the expression of genes involved in defense response, stress response, cell wall structure and chloroplast function, among others (Owens et al., 2017), ii) the direct interaction of viroid genomic RNA with host factors (Adkar-Purushothama and Perreault, 2020), and iii) the sequence-specific cleavage by viroid-derived small RNAs (vd-sRNAs) of complementary host mRNAs corresponding to genes involved in development, and iv) the induction of ribosomal stress (Cottilli et al., 2019). RNA-based resistance to viroids [reviewed in (Dalakouras et al., 2015; Flores et al., 2017)] has been achieved through the transgenic expression of antisense RNAs (Matousek et al., 1994), hammerhead ribozymes (Atkins et al., 1995; Yang et al., 1997; Carbonell et al., 2011), double-stranded RNA (dsRNA) ribonucleases (Sano et al., 1997) and hairpin RNAs of viroid sequence (Carbonell et al., 2008; Schwind et al., 2009; Adkar-Purushothama et al., 2015), or by exogenously applying to leaves large amounts of dsRNA molecules of viroid sequence (Carbonell et al., 2008). More recently, a large screening of multiple artificial microRNAs (amiRNAs) targeting sites distributed along viroid RNAs identified several amiRNAs that were highly active in agroinfiltrated leaves when co-expressed with an infectious viroid transcript (Carbonell and Daròs, 2017).

Plants contain three major species of sterols named β-sitosterol, stigmasterol and campesterol, and some members of the *Solanaceae* family also include important amounts of cholesterol (Moreau et al., 2002; Benveniste, 2004). Sterols accumulate in different forms, as free sterols (FSs) with a free β-hydroxyl group at C-3 position on the backbone, conjugated esters, sterol glycosides and acyl sterol glycosides. Sterol glycosides are

produced by UDP-glucose:sterol glycosyltransferases (SGTs) which catalyze the transfer of a glucose residue from UDP-glucose to the free hydroxyl group at position C-3 of FSs (Moreau et al., 2002; Benveniste, 2004). Sterols are important for regulating plant growth and development, as changes in cellular sterol composition affects a variety of cellular processes such as vascular and stomatal patterning, cell division, expansion and polarity, cell-to-cell connectivity and hormonal control among others (Ramirez-Estrada et al., 2017). Sterols are also key structural components of cellular membranes, regulate different membrane functions (e.g. passive or active transport across the membrane, activity of membranes associated with proteins, etc.), and changes in their relative proportion are known to alter membrane biophysical properties (Roche et al., 2008; Grosjean et al., 2015). Hence, sterols also play an important role in plant response to a diverse list of abiotic and biotic stresses including thermotolerance, drought, metal ions, H_2O_2 and bacterial or fungal pathogens. However, the role of sterols in plant defense against viruses or viroids is unknown (Altabella et al., 2022).

Here, we aimed to engineer tomato plants highly resistant to *Potato spindle tuber viroid* (PSTVd), the type species of the *Pospiviroidae* family (Gross et al., 1978). PSTVd naturally infects economically relevant crops such as potato (*Solanum tuberosum*) or tomato (*Solanum lycopersicum*), and is currently classified as a quarantine pathogen in certain regions of the world (Tsuda and Sano, 2014). A construct expressing a highly active anti-PSTVd amiRNA in *N. benthamiana* (Carbonell and Daròs, 2017) was introduced into tomato plants to generate multiple stably transformed lines that were analyzed for antiviroid resistance. Infectivity assays revealed, contrary to our expectations, that all amiRNA lines were hypersusceptible to PSTVd. A combination of phenotypic, molecular and metabolic analyses of several amiRNA-expressing lines non-inoculated with the viroid revealed that the amiRNA was accidentally silencing the tomato sterol 3-beta glycosyltransferase 1 (*SlSGT1*) gene, which caused late developmental and reproductive defects such as dwarfism, leaf epinasty and reduced fruit size and weight. Moreover, two independent transgenic tomato lines each expressing a different amiRNA specifically designed to target *SlSGT1* were also hypersusceptible to PSTVd, thus confirming that downregulation of *SlSGT1* was responsible of the hypersusceptibility phenotype.

MATERIALS AND METHODS

Plant materials and growing conditions

S. lycopersicum cv. Moneymaker Tm2 and cv. Micro-tom were grown in a growth chamber at 25ºC with a 12-light/12 h-dark photoperiod. Micro-tom transgenic lines expressing amiR-SlSGS1-1 or amiR-SlSGT1-2 amiRNAs were described elsewhere (Chávez et al., companion article).

DNA constructs

35S:amiR-PSTVd, *35S:amiR-SlSGT1-1* and *35S:amiR-SlSGT1-2* constructs were described previously (Carbonell and Daròs, 2017) (Chávez et al., companion article). The sequences of all amiRNA-generating precursors used in this study are listed in Supplemental Dataset 1.

Generation and phenotyping of tomato cv. Moneymaker transgenic plants

Agrobacterium tumefaciens LBA4404 transformed with *35S:amiR-PSTVd* was co-cultured with tomato cotyledons. Explant preparation, selection and regeneration were performed as described (Ellul et al., 2003). Transformants were selected in hygromycin-containing medium, and then propagated in soil for seed production and for the infection studies. Non-transgenic controls (NTC) were *in vitro*-regenerated tomato plants obtained in parallel with the transgenic plants. Phenotyping analyses were done using four NTCs and four independent amiRNA lines.

Viroid infection assays

A CF11 cellulose-treated RNA extract was obtained from *N. benthamiana* tissue infected with PSTVd RG1 strain (GenBank Acc. No. U23058). Tomato plants were inoculated by mixing 5 µL of the infectious extract with 5 µL of a 10% carborundum solution (in 50 mM K_2HPO_4) in one leaf while evenly spreading the inoculum with a glass rod. After inoculation,

plants were monitored for viroid symptom appearance throughout four weeks. The two youngest leaves were sampled for RNA preparation and analysis.

RNA preparation

Total RNA from *S. lycopersicum* leaves was isolated in extraction buffer (1 M guanidinium thiocyanate, 1 M ammonium thiocyanate, 0.1 M sodium acetate, 5 % glycerol, 38 % water saturated phenol), followed by chloroform extraction. RNA was precipitated in 0.5X isopropanol for 20 min. Triplicate samples from pools of two leaves were analyzed.

Real-time RT-qPCR

Real-time RT-qPCR was done essentially as described (López-Dolz et al., 2020) in a QuantStudio 3 Real-Time PCR System (Thermo Fisher Scientific). Primers used for RT-qPCR are listed in Supplemental Table 1. Target RNA expression levels were calculated relative to two *S. lycopersicum* reference genes (*SlACT* and *SlEXP*) using the delta delta cycle threshold comparative method of the QuantStudio Design and Analysis Software (version 1.5.1.; Thermo Fisher Scientific).

Small RNA blot assays

Total RNA (20 µg) was separated in 17% polyacrylamide gels containing 0.5 x Tris/Borate EDTA (TBE) and 7 M urea and transferred to positively charged nylon membrane. Probe synthesis using [γ-^{32}P]ATP (PerkinElmer) and T4 polynucleotide kinase (Thermo Fisher Scientific) and Northern-blot hybridizations were done at 38ºC in PerfectHyb Plus Hybridization Buffer (Sigma-Aldrich) as described (Montgomery et al., 2008; Carbonell et al., 2014). A Typhoon IP Imager System (Cytiva) was used to produce digital images from radioactive membranes. Oligonucleotides used as probes for sRNA blots are listed in Supplemental Table 1.

5'-RLM-RACE

RNA ligase-mediated rapid amplification of 5' cDNA ends was done using the GeneRacer kit (Life Technologies) as described (Carbonell et al., 2015), except that the 5' end of cDNA specific to *SlSGT1* was directly amplified in a single PCR using the GeneRacer 5' and gene-specific AC-569 oligonucleotides. 5' RLM-RACE products were gel purified and cloned using the Zero Blunt TOPO PCR Cloning Kit (Life Technologies), introduced in *Escherichia coli* DH5α, screened for inserts, and sequenced. Control PCR reactions to amplify *SlACT* were done using oligonucleotides AC-280 and AC-281 done. The sequences of the oligonucleotides used are listed in Supplemental Table 1.

Sterol analysis

For leaf sterol measurements, a pool of two apical leaves from four NTC and four amiR-PSTVd independent *S. Lycopersicum* lines was analyzed. Sterols were extracted and quantified by GC-MS in three technical replicates for each genotype (n=3), as previously described (Ramirez-Estrada et al., 2017).

RNA sequencing and data analysis

Total RNA from four wild-type and four amiR-PSTVd independent *S. Lycopersicum* lines was analyzed for quantity, purity and integrity with a 2100 Bioanalyzer (RNA 6000 Nano kit; Agilent), and submitted to BGI (Hong Kong, China) for strand-specific library preparation and mRNA sequencing in DNBSEQ Platform. After quality analysis with FastQC (https://www.bioinformatics.babraham.ac.uk/projects/fastqc/), and adapter removal and low-quality trimming of raw reads with cutadapt (Martin, 2011), clean read pairs were mapped to *S. lycopersicum* genome (version 4.0) using HISAT2 (Kim et al., 2015), and non-uniquely mapped pairs were discarded. Number of read counts uniquely mapped to each tomato gene were obtained with htseq-count (Anders et al., 2015) using the iTAG4.0 gene model annotation. Genes not having at least 1 TPM (Transcripts Per Kilobase per Million mapped reads), in either the four wild type replicates or the four amiR-PSTVd lines, were

filtered out. Differential expression analysis was done with DESeq2 (Love *et al.*, 2014), with a false discovery rate of 1%. Differential gene expression analysis results are shown in Supplemental Dataset 2. MA plot was generated using ggplot2 (Wickham 2016) in RStudio (https://www.rstudio.com/). Gene ontology analysis was done using ShinyGo v0.75 (http://bioinformatics.sdstate.edu/go/) (Ge et al., 2020) with a false discovery rate of 5%.

Off-target analysis

TARGETFINDER v1.7 (https://github.com/carringtonlab/TargetFinder) (Fahlgren and Carrington, 2010) was used to obtain a ranked list of potential off-targets for amiR-PSTVd (Supplemental Dataset 3) .

Accession numbers

S. lycopersicum genes and corresponding locus identifiers are: *SlACT* (*Solyc04g011500.3*), *SlEXP* (SGN-U346908), *SlSGT1* (*Solyc06g007980.4*), *SlNAC082* (*Solyc11g005920.1*), *SlPR1* (X71592.1). High-throughput sequencing data from this article can be found in the Sequence Read Archive (SRA) database under the accession number PRJNA849770.

RESULTS

Transgenic tomato plants expressing an amiRNA against PSTVd are hypersusceptible to viroid infection

A construct expressing a highly effective anti-PSTVd amiRNA selected from a previous functional screening in *Nicotiana benthamiana* (Carbonell and Daròs, 2017) was introduced in *S. lycopersicum* cv. Moneymaker (Figure 1A). Eight independent transgenic T1 lines were generated, all of them with a phenotype that was indistinguishable from that of non-transgenic control (NTC) tomato plants at 10 days post transplanting (Figure 1B). Northern blot analysis of RNA preparations obtained from apical leaves revealed that all lines

accumulated amiR-PSTVd to similar levels (Figure 1C). Four of the lines (#1, #2, #5 and #16) were selected for further analyses.

To analyze the antiviroid resistance of each independent line, three individuals (propagated from cuttings) of each transgenic line were inoculated with PSTVd. In parallel, three NTC plants were mock- or PSTVd-inoculated. The appearance of typical PSTVd symptoms (leaf epinasty and chlorosis) in distant non-inoculated tissues was recorded during four weeks post inoculation (wpi). Surprisingly, amiRNA plants displayed symptoms earlier than NTC plants (Figure 2A). For instance, 37.5 % of amiRNA plants showed symptoms as early as 11 days post inoculation (dpi), and 100 % at 13 dpi. In contrast, first symptoms in NTC plants were observed in 50 % of the plants at 13 dpi, and only at 14 dpi all the NTC plants were symptomatic (Figure 2A). At the end of the experiment (4 wpi), PSTVd-infected amiRNA lines were clearly shorter than NTC plants (Figure 2B).

PSTVd accumulation was analyzed by reverse transcription followed by quantitative polymerase chain reaction (RT-qPCR) in selected amiRNA lines and NTCs at two different time points, 2 and 4 wpi (Figure 2C). At 2 wpi, PSTVd accumulated to significantly lower levels in all amiRNA lines compared to infected NTCs, suggesting that amiR-PSTVd interferes with viroid infection, as predicted. However, this protective effect was transient because at 4 wpi PSTVd accumulation was similar in all infected plants (Figure 2C). Importantly, the loss of the effect was not due to a decrease in amiR-PSTVd levels at later stages of infection, as amiR-PSTVd accumulated to similar levels at the two time points (Supplemental Figure 1). Because viroid symptomatology in tomato positively correlates with the expression of pathogenesis related (PR) proteins such as pathogenesis related protein 1 (PR1) and ribosomal stress inducing factors such as NAC082 (Cottilli et al., 2019; Vázquez Prol et al., 2021), the accumulation of *SlPR1* and *SlNAC082* mRNAs was analyzed in all plants (Figure 2C). As expected, at 2 wpi both *SlPR1* and *SlNAC082* were induced in infected NTCs compared to mock NTCs. Interestingly, at this same time point *SlPR1* and *SlNAC082* accumulated to significantly higher levels in all amiRNA lines. Similar results were obtained at 4 wpi, although the increase of *SlPR1* and *SlNAC082* levels in amiRNA lines versus NTCs was more modest. All together, these results indicate that amiR-PSTVd-expressing lines are hypersusceptible to viroid infection. They also reveal that *SlPR1* and *SlNAC082* are induced in PSTVd-infected plants to levels that correlate with viroid symptomatology.

AmiR-PSTVd-expressing lines display late developmental defects

In parallel, NTCs and amiRNA lines were also grown for seed propagation in greenhouse conditions. Unexpectedly, around 6 weeks post transplanting (wpt) the *in vitro* plantlets, all amiRNA lines showed slight dwarfing and leaf curling that became obvious at 8 wpt (Figure 3A). Mean height of amiRNA plants was significantly reduced (1.9 fold) compared to NTCs (Figure 3B, top), and internode length of amiRNA lines was also significantly reduced compared to that of NTCs (Figure 3B, bottom). Moreover, tomato fruits from amiRNA lines were significantly smaller and had a lower fresh weight than fruits from NTCs (Figure 3C and D). In conclusion, amiR-PSTVd expressing lines showed obvious developmental defects at later stages of growth including dwarfism, leaf epinasty and reduced fruit size and weight.

Transcriptome profiling combined with RT-qPCR, 5'RLM-RACE, and metabolomic analyses reveal that endogenous UDP-glucose:sterol glycosyl transferase 1 is down-regulated in amiR-PSTVd-expressing lines

The unexpected phenotype of the tomato transgenic lines prompted us to hypothesize that amiR-PSTVd might be accidentally targeting (and down-regulating) one or more endogenous transcripts involved in the induction of the observed late developmental defects. We reasoned that, if existing, putative off-target(s) of amiR-PSTVd would have a high sequence complementarity with the amiRNA and be differentially underexpressed in amiR-PSTVd-expressing lines.

To reveal the identity of the putative off-target(s), first we used TargetFinder tool (Fahlgren and Carrington, 2010) to generate a genome-wide list of all targets sharing a relatively high sequence complementarity with amiR-PSTVd (Supplemental Dataset 3). TargetFinder predicted off-targets are ranked based on a Target Prediction Score (TPS) assigned to each amiRNA-target interaction. TPS ranges from 1 to 11, that is from highest to lowest degree of complementarity between the amiRNA and the putative target RNA. Indeed, amiR-PSTVd was designed with "P-SAMS amiRNA Designer" tool (Fahlgren et al., 2016) because none of the interactions between amiR-PSTVd and cellular RNAs had a TPS<4,

which is the arbitrary cut off that P-SAMS uses to assign high specificity to the designed amiRNA. However, we cannot completely rule out that amiR-PSTVd-target RNA interactions with a TPS>4 may be productive and lead to the downregulation of the corresponding target RNA. Table 1 lists amiR-PSTVd most probable off-target transcripts with a TPS ≤ 6 based on TargetFinder analysis.

Next, transcript libraries from four NTCs and four amiR-PSTVd-expressing lines were generated and analyzed. Differential gene expression analysis was done by comparing the transcript libraries from the NTCs with those from the amiR-PSTVd expressing lines. In total, 223 genes were differentially expressed in plants expressing amiR-PSTVd, with 176 genes being differentially overexpressed and 47 differentially underexpressed (Figure 4A, Supplemental Dataset 2). Interestingly, *Solyc06g007980.4* was the only differentially underexpressed gene included in the list of most probable off-targets (Table 1). Indeed, this gene was the fifth most differentially underexpressed (Supplemental Dataset 2) and the third potential off-target with lowest TPS (Supplemental Dataset 3). This gene encodes the tomato sterol 3-beta glycosyltransferase 1 (*SlSGT1*), one of the four isoenzymes that catalyzes the glycosylation of the free hydroxyl group at C-3 position of sterols to produce sterol glycosides in tomato (Ramirez-Estrada et al., 2017). RT-qPCR analyses confirmed that *SlSGT1* mRNA accumulated to significantly lower levels in amiRNA-expressing lines compared to NTCs (Figure 4B). Next, we used RNA ligase-mediated rapid amplification of 5' cDNA ends (5' RLM-RACE) to test for amiR-PSTVd-directed off-target cleavage of *SlSGT1*. If amiR-PSTVd is cleaving *SlSGT1* mRNA, this analysis will detect the 3' cleavage products. Such cleavage products of the expected size (439 bp) were detected in samples expressing amiR-PSTVd, but not in NTC samples. Sequencing analysis confirmed that the majority (6/7) of the sequences comprising these products contained the canonical 5' end position predicted for amiR-PSTVd-guided cleavage (Figure 4C).

Finally, sterol glycosides and free sterol forms (SGs and FSs, respectively) for the main tomato sterol species (cholesterol, campesterol, stigmasterol and β-sitosterol) were analyzed and quantified in both NTC and amiRNA transgenic lines (Supplemental Table 2). As expected from *SlSGT1* downregulation, the content of bulk sterol glycosides was significantly reduced by about 50% in amiRNA lines compared to NTCs (Figure 4D). Conversely, the content of major free sterols was significantly increased in amiRNA lines

(Figure 4D), thus confirming the reduced glycosylation activity in *SlSGT1*-silenced amiRNA lines. All together, these results indicate that amiR-PSTVd is downregulating *SlSGT1*, which affects sterol glycosylation and most likely causes the late developmental defects observed in the tomato transgenic lines.

Is *SlSGT1* a direct target of PSTVd during infections?

Notably, the late development defects of the amiRNA lines resembled the symptomatology observed in natural PSTVd infections. Thus, we hypothesized that *SlSGT1* might be targeted during PSTVd infection in tomato and that *SlSGT1* down-regulation may be, at least in part, responsible for the developmental defects observed in natural PSTVd infections. Because vd-sRNAs are known to associate with ARGONAUTE (AGO) proteins to target host genes (Navarro et al., 2021a), we thought that maybe vd-sRNAs with sequence similar to amiR-PSTVd may exist in natural PSTVd infections, associate with AGO1 and target *SlGST1*. Thus, we searched public high-throughput sRNA sequencing data and found three PSTVd-derived sRNAs of (-) polarity with high sequence similarity with amiR-PSTVd (Figure 5A), and that were in the top ten of most highly enriched vd-sRNAs in AGO1 immunoprecipitated fractions from *N. benthamiana* tissue infected with PSTVd (Minoia et al., 2014). Still, the lowest TPS from the interactions between PSTVd-sRNAs and *SlGST1* corresponded to PSTVd-sRNA (-) (261-281) with a relatively high score of 8. 5'RLM-RACE analysis confirmed that *SlSGT1* 3' cleavage products could only be detected in infected transgenic lines expressing amiR-PSTVd, but not in infected NTCs (Figure 5B). Also, we observed that *SlSGT1* mRNA accumulation in NTC plants infected with PSTVd was not significantly different from that of mock-inoculated NTCs (Figure 5C). Still, it is possible that *SlSGT1* mRNA accumulation remains unaltered because down-regulation by a putative PSTVd-sRNA may be compensated by an induction of *SlSGT1* transcription upon viroid infection. Thus, we also performed RT-qPCR with *SlSGT1* intron-specific primers and found that *SlSGT1* primary transcripts accumulate to similar levels in mock and PSTVd infected NTC plants (Supplemental Figure 2). These results suggest that *SlSGT1* expression is not induced in PSTVd-infected plants. Taken together, our results do not support that *SlSGT1* may be a direct target in natural PSTVd infections in tomato.

Transgenic tomato plants expressing an amiRNA specifically designed against *SlSGT1* are also hypersusceptible to viroid infection

To confirm that downregulation of *SlSGT1* induces hypersusceptibility to PSTVd, two transgenic *S. lycopersicum* cv. Micro-Tom lines expressing amiR-SGT1-1 or amiR-SGT1-2 amiRNAs specifically designed to target *SlSGT1* (Figure 6A) were challenged with PSTVd. In particular, three individuals of each transgenic line and three NTCs were inoculated with PSTVd, and three other NTC were mock inoculated. Plant response to PSTVd infection was analyzed as before, that is recording the day of symptom appearance of each plant and analyzing the accumulation of PSTVd, and of *SlPR1* and *SlNAC082* mRNAs at 2 and 4 wpi. As a control, accumulation of *SlSGT1* was also analyzed at the same time points.

As for amiR-PSTVd lines, both amiR-SGT1-expressing lines displayed symptoms earlier than NTC plants (Figure 6B). For example, 75 % of amiR-SGT1-1 and 100 % of amiR-SGT1-2 plants showed symptoms as early as 10 dpi. In contrast, first symptoms in NTC plants were observed in 50 % of the plants at 12 dpi, and only at 13 dpi all the NTC plants were symptomatic (Figure 6B). At the end of the experiment (4 wpi), both PSTVd-infected amiR-SGT1 lines were clearly dwarfer than NTC plants (Figure 6C). RT-qPCR analysis showed that PSTVd accumulation was similar in all infected plants, both at 2 and 4 wpi, while accumulation of *SlPR1* and *SlNAC082* mRNAs was significantly higher in both amiR-SGT1 lines compared to NTCs at the two time points (Figure 6D). Finally, *SlSGT1* mRNA accumulation was significantly reduced in both amiR-SGT1 lines compared to NTCs both in the absence or presence of PSTVd (Figure 6D).

DISCUSSION

In this work, several *S. lycopersicum* cv Moneymaker transgenic lines expressing an amiRNA against PSTVd (amiR-PSTVd) were generated. Phenotypic and molecular analyses revealed, contrary to our expectations, that amiR-PSTVd-expressing lines were not resistant but rather hypersusceptible to the viroid. Intriguingly, non-infected amiR-PSTVd lines showed late developmental defects including leaf epinasty, dwarfism and fruit size and weight reduction, which are also typical of PSTVd infection. A combination of transcriptome

profiling with RT-qPCR, 5'RLM-RACE, and metabolomic analyses revealed that these phenotypic defects were caused by the accidental downregulation of endogenous *SlGST1* by amiR-PSTVd-expressing lines.

SlSGT1 is required for proper plant and fruit development in tomato

Previous works indicate that a proper balance between the levels of GSs and FSs is crucial for normal cell function and plant development. For instance, the ugt80A2,B1 Arabidopsis double mutant that accumulates low GSs levels displays diverse morphological and biochemical seed phenotypes (DeBolt et al., 2009), alterations in the male gametophyte (Choi et al., 2014) and aberrant root epidermal cell patterning (Pook et al., 2017). In our work, downregulation of *SlGST1* in amiR-PSTVd-expressing tomato plants induces late development phenotypes such as leaf epinasty, dwarfing and reduced fruit size, similarly to the phenotypes described in amiR-SGT1-expressing tomato plants (Chávez et al. companion article). Shortened plant height and leaf area was previously observed in *Withania somnifera* plants transiently expressing a VIGS construct against endogenous *SGTs* (Singh et al., 2016) while *W. somnifera SGT1* over-expression caused enhanced growth and expansion of leaves (Saema et al., 2016), thus reinforcing the idea of the essential role of SGTs in proper plant development. Here, as observed in our metabolic analyses, down-regulation of *SlSGT1* causes imbalance of GSs and FSs which might alter membrane biophysical properties and negatively affect the function of membrane-bound proteins such as the receptors of the plant hormones cytokinins, ethylene and brassinosteroids –known to be membrane-localized proteins (Takeuchi et al., 2021). The interference with hormone receptor function might affect the growth hormone signaling pathway which could hinder the growth of amiR-PSTVd plants. Indeed, the dwarfing and leaf epinasty phenotype observed in the amiR-PSTVd lines is typical of plants affected in brassinosteroid signaling (Zhu et al., 2013; Carbonell et al., 2015). Still, the significantly higher levels of free campesterol, the main precursor of brassinosteroids, in amiR-PSTVd lines (Supplemental Figure 3) suggest that brassinosteroid biosynthesis may not be negatively affected at least by the altered campesterol levels.

On the other hand, a gene ontology analysis on our RNA-seq data revealed that several cellular component categories related with membranes were significantly altered (Supplemental Figure 4, Supplemental Dataset 4), which is not surprising based on the important roles of sterols in cellular membranes. Moreover, we identified several cytochrome P450-encoding genes that were misregulated (Supplemental Dataset 2). As cytochrome P450 are membrane-bound monooxygenases, the alteration of membranes due to *SlGST1* downregulation may also directly affect the stability of such enzymes. Interestingly, several cytochrome P450 enzymes catalyze essential oxidative reactions in the biosynthesis or catabolism of several plant hormones such as brassinosteroids, abscisic acid, jasmonyl-isoleucine or strigolactones (Bak et al., 2011). Pertinent to this context, our RNA-seq data indicates that CYP722 cytochrome P450 (*Solyc02g084930*) involved in brassinosteroid biosynthesis (Fujioka and Yokota, 2003; Nelson and Werck-Reichhart, 2011) is significantly down-regulated in amiR-PSTVd lines, while CYP707A1 (*Solyc08g005610*) and CYP94B3/CYP94C1 (*Solyc03g111290*/ *Solyc06g074420*) participating in abscisic acid catabolism (Okamoto et al., 2006) and in jasmonyl-isoleucine inactivation and attenuation of the jasmonic acid signaling cascade (Bruckhoff et al., 2016) respectively, are up-regulated in these same lines (Supplemental Dataset 2). Thus, it cannot be ruled out that altered cytochrome P450 balances may affect hormone biosynthesis or catabolic pathways. In any case, future research is needed to better dissect the effect of cellular membrane destabilization (due to reduced sterol glycosylation) with the stability of membrane components as well as the specific contribution of alterations in diverse hormone pathways in the phenotype of amiR-PSTVd lines.

Viroid symptoms positively correlate with *SlPR1* and *SlNAC082* expression levels but not with viroid titer

Interestingly, both amiR-PSTVd- and amiR-SlSGT1-expressing plants showing more severe symptoms than NTCs accumulate similar or lower levels of PSTVd at 2 and 4 wpi (Figures 2C and 6D). These data indicate that symptom development is not correlated with PSTVd accumulation. Although this result might seem surprising, this observation was already reported in experiments comparing the degree of symptoms induced by different PSTVd strains in tomato plants (Gruner et al., 1995), and more recently also in *N. benthamiana*,

Prunus persica (peach) and tomato plants infected *Hop stunt viroid* (HSVd) (Gomez et al., 2008), *Peach latent mosaic viroid* (PLMVd) (Rodio et al., 2006) or with CEVd (Vázquez Prol et al., 2020), respectively. In any case, our results suggest that viroid-induced symptoms in distant tissues depend on the viroid presence but do not correlate with viroid titer. This could indicate that symptom development in distant tissues may be triggered when a certain amount of viroid accumulates in this tissue above a threshold but is not enhanced by further viroid accumulation.

Viroids trigger plant's defense responses and induce the expression of pathogenesis related (PR) proteins such as PR1 (Granell et al., 1987; Lisón et al., 2013), whose induction in tomato correlates with viroid-induced symptomatology as observed for several viroids (Vázquez Prol et al., 2021). Recently, the induction of the ribosomal stress mediator *SlNAC082* was observed upon CEVd infection in tomato and correlated with viroid-induced symptoms (Cottilli et al., 2019; Vázquez Prol et al., 2020), indicating that viroids can induce alterations in the biogenesis of ribosomes. Here, both *SlPR1* and *SlNAC082* are induced in PSTVd-infected NTCs and significantly overinduced in amiR-PSTVd- or amiR-SlGST1-expressing plants infected with PSTVd (Figure 2C and 6D).

Viroid movement may be facilitated in *SlSGT1*-silenced plants

During infections, viroids move from inoculated to distal tissues where symptoms like leaf epinasty and chlorosis are developed. Viroid movement includes intracellular movement (and subcellular compartmentalization for replication), exit of viroid progeny to neighboring cells and entry to vascular tissue for long-distance trafficking (Pallás and Gómez, 2017). For instance, viroids can move from cell to cell via plasmodesmata, as shown years ago for PSTVd in tomato and tobacco mesophyll (Ding et al., 1997). Our results show that *SlGST1* downregulation impacts the cellular sterol profile (Supplemental Table 2), with a decrease in SGs and an increase in FSs (Figure 4D). Because SGs and FSs are primary structural elements of cell membranes (Roche et al., 2008; Grosjean et al., 2015), it is possible that cytoplasmic membranes are altered in *SlSGT1*-silenced plants. This could affect membrane permeability and fluidity and somehow facilitate viroid cell to cell and long-distance transit through plasmodesmata, whose correct function depends on a specific

membrane composition of lipids including sterols (Grison et al., 2015). Indeed, cytopathic effects at the plasma membrane in association with CEVd in infected *Gynura aurantiaca* were described more than four decades ago (Semancik and Vanderwoude, 1976). Also, to be noted is that viroid systemic infections generally take several weeks and are slow when compared to virus counterparts infecting the same hosts, as viruses usually reach distal tissues in just a few days. This could be related to viroid steric difficulties to transit the plasmodesmata in the absence of movement proteins, such as those encoded in plant virus genomes that facilitates the process. It is tempting to speculate that the sterol unbalance may disturb plasmodesmal control, which could be used by viroids to move faster cell to cell through plasmodesmata in infected tissues. In this scenario, PSTVd may reach distant tissues more rapidly in *SlSGT1*-silenced plants to incite symptoms earlier than in wild-type plants. This could explain why symptom development is accelerated in *SlSGT1*-silenced plants (Figure 7). Still, our RT-qPCR and 5'-RLM-RACE analyses in PSTVd-infected NTCs could not prove that *SlSGT1* is a direct target of PSTVd in natural infections. A close examination of recently published degradome datasets from PSTVd-infected tomato and *N. benthamiana* failed to identify degradome signatures of *SlSGT1* mRNAs by PSTVd-sRNAs (Navarro et al., 2021b). Still, it is possible that both PSTVd-sRNAs and *SlSGT1* mRNAs may be accumulating in a non-uniform manner in tomato tissues so that cleaving of *SlSGT1* mRNAs might occur only in a subset of tissues. In this scenario, mRNA cleavage would be more difficult to detect than in the amiR-PSTVd plants, where amiRNA expression occurs in most (if not all) cells. Also, *SlSGT1* silencing may only need to occur in certain cell types to induce PSTVd-like phenotypes. Finally, it is also possible that PSTVd-sRNAs could block *SlSGT1* translation or epigenetically regulate *SlSGT1* expression, or that other *SlSGT* isoforms could be regulated upon natural viroid infections. For all these reasons we cannot rule out the possibility that *SlSGT1* could be a direct target of PSTVd during natural infections.

Roles of SGTs in stress response

SGTs have been recently linked to enhanced salt stress resistance, as reported for Arabidopsis plants overexpressing *Whitania somnifera* SGT gene (Mishra et al., 2021). The role of SGTs in biotic stress response has also been reported in several plant species. While silencing of several members of the *SGT* gene family led to a decrease in *Withania somnifera* basal immunity against *Alternaria alternata* (Singh et al., 2016), overexpression of *W.*

somnifera SGT in Arabidopsis and tobacco plants showed increased resistance against *Alternaria brassicicola* and *Spodoptera litura*, respectively (Pandey et al., 2014; Mishra et al., 2017). In these reports, it is still not known if the resistance effects were due to the modified levels of SGs or were induced by the concomitant changes observed for other plant defense compounds. Pertinent to this observation, it was also described that resistance against the bacterial necrotrophy *Botrytis cinerea* is enhanced in Arabidopsis ugt80A2;B1 double mutant which is impaired in SG biosynthesis. In this case the resistance phenotype was explained by the transcriptional and metabolic changes induced by an increase in jasmonic acid and camalexin levels observed in this double mutant (Castillo et al., 2019).

Sterols have also been linked with plant virus replication [(for a recent review see (Altabella et al., 2022)], as the formation of viral replication complexes involves the recruitment of high levels of sterols. Moreover, it is known that the inhibition of sterol biosynthesis reduces tombusvirus replication in yeast and plants (Sharma et al., 2010). Also, it is possible that modifying the sterol profiles of a plant could ultimately increase its antiviral resistance, as suggested before (Altabella et al., 2022). Therefore, our amiR-PSTVd or amiR-SlSGT1 plants could be a very useful tool to assess in future experiments if low *SlSGT1* levels induce enhanced antiviral resistance in tomato. Still, a better understanding of the impact of sterol profiles in biophysical properties of cellular membranes, and of the specific role of GSs predominant in *Solanaceae* species will facilitate the development of enhanced antiviral resistance for next-generation crops.

ACKNOWLEDGEMENTS

We would like to thank Javier Forment (IBMCP) for helping in the RNAseq data analysis and the greenhouse staff of IBMCP for the maintenance of plants.

CONFLICTS OF INTEREST

The authors declare no conflicts of interest.

FUNDING

This work was supported by grants from Ministerio de Ciencia e Innovación (MCIN, Spain), Agencia Estatal de Investigación (AEI, Spain) and Fondo Europeo de Desarrollo Regional (FEDER, European Union) (RTI2018-095118-A-100 and RYC-2017-21648 to A.C, PRE2019-088439 to AEC, PIE2020-116765RB-I00 to P.L. and PID2020-114691RB-I00 to J.-A.D, AGL2017-88842-R to AF and TA, and Severo Ochoa Programme for Centres of Excellence in R&D CEX2019-000902-S), Generalitat Valenciana (PROMETEU/2021/056 to P.L.), Generalitat de Catalunya (2017SGR710 and CERCA Programme).

AUTHORS CONTRIBUTIONS

AEC and AC performed most of the experimental work. PL and LC generated and maintained the tomato cv. Moneymaker amiR-PSTVd transgenic plants. JML-T, TA and AF performed the sterol analysis. JAD participated in the original conception of the project. AC conceived the research, supervised the project and wrote the manuscript.

DATA AVAILABILITY STATEMENT

All data relating to this manuscript can be found within the manuscript and its supplementary files. Data that support the findings of this study are available from the corresponding author upon reasonable request. High-throughput sequencing data can be found in the Sequence Read Archive (SRA) database under accession number PRJNA849770.

REFERENCES

Adkar-Purushothama CR, Kasai A, Sugawara K, Yamamoto H, Yamazaki Y, He YH, Takada N, Goto H, Shindo S, Harada T, et al (2015) RNAi mediated inhibition of viroid infection in transgenic plants expressing viroid-specific small RNAs derived from various functional domains. Scientific Reports **5**: 17949

Adkar-Purushothama CR, Perreault J-P (2020) Current overview on viroid–host interactions. WIREs RNA **11**: e1570

Altabella T, Ramirez-Estrada K, Ferrer A (2022) Phytosterol metabolism in plant positive-strand RNA virus replication. Plant Cell Reports **41**: 281–291

Anders S, Pyl PT, Huber W (2015) HTSeq—a Python framework to work with high-throughput sequencing data. Bioinformatics **31**: 166–169

Atkins D, Young M, Uzzell S, Kelly L, Fillatti J, Gerlach WL (1995) The expression of antisense and ribozyme genes targeting citrus exocortis viroid in transgenic plants. The Journal of general virology **76 (Pt 7)**: 1781–90

Bak S, Beisson F, Bishop G, Hamberger B, Höfer R, Paquette S, Werck-Reichhart D (2011) Cytochromes P450. arbo.j. doi: 10.1199/tab.0144

Benveniste P (2004) Biosynthesis and Accumulation of Sterols. Annual Review of Plant Biology **55**: 429–457

Branch AD, Robertson HD (1984) A replication cycle for viroids and other small infectious RNA's. Science (New York, NY **223**: 450–5

Bruckhoff V, Haroth S, Feussner K, König S, Brodhun F, Feussner I (2016) Functional Characterization of CYP94-Genes and Identification of a Novel Jasmonate Catabolite in Flowers. PLOS ONE **11**: e0159875

Carbonell A, Daròs J-A (2017) Artificial microRNAs and synthetic trans-acting small interfering RNAs interfere with viroid infection. Molecular Plant Pathology **18**: 746–753

Carbonell A, Fahlgren N, Mitchell S, Cox KL Jr, Reilly KC, Mockler TC, Carrington JC (2015) Highly specific gene silencing in a monocot species by artificial microRNAs derived from chimeric miRNA precursors. Plant Journal **82**: 1061–75

Carbonell A, Flores R, Gago S (2011) Trans-cleaving hammerhead ribozymes with tertiary stabilizing motifs: in vitro and in vivo activity against a structured viroid RNA. Nucleic Acids Research **39**: 2432–44

Carbonell A, Martinez de Alba AE, Flores R, Gago S (2008) Double-stranded RNA interferes in a sequence-specific manner with the infection of representative members of the two viroid families. Virology **371**: 44–53

Carbonell A, Takeda A, Fahlgren N, Johnson SC, Cuperus JT, Carrington JC (2014) New generation of artificial MicroRNA and synthetic trans-acting small interfering RNA vectors for efficient gene silencing in Arabidopsis. Plant Physiology **165**: 15–29

Castillo N, Pastor V, Chávez Á, Arró M, Boronat A, Flors V, Ferrer A, Altabella T (2019) Inactivation of UDP-Glucose Sterol Glucosyltransferases Enhances Arabidopsis Resistance to Botrytis cinerea. Frontiers in Plant Science **10**: 1162

Chávez Á, Castillo N, López-Tubau JM, Atanasov KE, Fernández-Crespo E, Camañes G, Altabella T, Ferrer A. Tomato *STEROL GLYCOSYLTRANSFERASE 1* Unveils a Major Role of Steryl Glycosydes in Plant and Fruit Development. Companion article submitted to Journal of Experimental Botany.

Choi H, Ohyama K, Kim Y-Y, Jin J-Y, Lee SB, Yamaoka Y, Muranaka T, Suh MC, Fujioka S, Lee Y (2014) The Role of Arabidopsis ABCG9 and ABCG31 ATP Binding Cassette Transporters in Pollen Fitness and the Deposition of Steryl Glycosides on the Pollen Coat. The Plant Cell **26**: 310–324

Cottilli P, Belda-Palazón B, Adkar-Purushothama CR, Perreault J-P, Schleiff E, Rodrigo I, Ferrando A, Lisón P (2019) Citrus exocortis viroid causes ribosomal stress in tomato plants. Nucleic Acids Research **47**: 8649–8661

Dalakouras A, Dadami E, Wassenegger M (2015) Engineering viroid resistance. Viruses **7**: 634–46

Daros JA (2016) Viroids: small noncoding infectious RNAs with the remarkable ability of autonomous replication. *In* A Wang, X Zhou, eds, Current Research Topics in Plant Virology. Springer International Publishing, pp 295–321

DeBolt S, Scheible W-R, Schrick K, Auer M, Beisson F, Bischoff V, Bouvier-Navé P, Carroll A, Hematy K, Li Y, et al (2009) Mutations in UDP-Glucose:Sterol Glucosyltransferase in Arabidopsis Cause Transparent Testa Phenotype and Suberization Defect in Seeds. Plant Physiology **151**: 78–87

Ding B, Kwon M-O, Hammond R, Owens R (1997) Cell-to-cell movement of potato spindle tuber viroid. The Plant Journal **12**: 931–936

Ellul P, Garcia-Sogo B, Pineda B, Rios G, Roig LA, Moreno V (2003) The ploidy level of transgenic plants in Agrobacterium-mediated transformation of tomato cotyledons (Lycopersicon esculentum Mill.) is genotype and procedure dependent [corrected]. Theoretical and Applied Genetics **106**: 231–8

Fahlgren N, Carrington JC (2010) miRNA Target Prediction in Plants. Methods in molecular biology **592**: 51–7

Fahlgren N, Hill ST, Carrington JC, Carbonell A (2016) P-SAMS: a web site for plant artificial microRNA and synthetic trans-acting small interfering RNA design. Bioinformatics **32**: 157–8

Flores R, Hernandez C, Martinez de Alba AE, Daros JA, Di Serio F (2005) Viroids and viroid-host interactions. Annual review of phytopathology **43**: 117–39

Flores R, Minoia S, Carbonell A, Gisel A, Delgado S, Lopez-Carrasco A, Navarro B, Di Serio F (2015) Viroids, the simplest RNA replicons: How they manipulate their hosts for being propagated and how their hosts react for containing the infection. Virus Research **209**: 136–45

Flores R, Navarro B, Kovalskaya N, Hammond RW, Di Serio F (2017) Engineering resistance against viroids. Current Opinion in Virology **26**: 1–7

Fujioka S, Yokota T (2003) Biosynthesis and Metabolism of Brassinosteroids. Annual Review of Plant Biology **54**: 137–164

Ge SX, Jung D, Yao R (2020) ShinyGO: a graphical gene-set enrichment tool for animals and plants. Bioinformatics **36**: 2628–2629

Gomez G, Martinez G, Pallas V (2008) Viroid-induced symptoms in Nicotiana benthamiana plants are dependent on RDR6 activity. Plant physiology **148**: 414–23

Granell A, Bellés JM, Conejero V (1987) Induction of pathogenesis-related proteins in tomato by citrus exocortis viroid, silver ion and ethephon. Physiological and Molecular Plant Pathology **31**: 83–90

Grison MS, Brocard L, Fouillen L, Nicolas W, Wewer V, Dörmann P, Nacir H, Benitez-Alfonso Y, Claverol S, Germain V, et al (2015) Specific Membrane Lipid Composition Is Important for Plasmodesmata Function in Arabidopsis. The Plant Cell **27**: 1228–1250

Grosjean K, Mongrand S, Beney L, Simon-Plas F, Gerbeau-Pissot P (2015) Differential Effect of Plant Lipids on Membrane Organization: SPECIFICITIES OF PHYTOSPHINGOLIPIDS AND PHYTOSTEROLS*. Journal of Biological Chemistry **290**: 5810–5825

Gross HJ, Domdey H, Lossow C, Jank P, Raba M, Alberty H, Sanger HL (1978) Nucleotide sequence and secondary structure of potato spindle tuber viroid. Nature **273**: 203–8

Gruner R, Fels A, Qu F, Zimmat R, Steger G, Riesner D (1995) Interdependence of Pathogenicity and Replicability with Potato Spindle Tuber Viroid. Virology **209**: 60–69

Kim D, Langmead B, Salzberg SL (2015) HISAT: a fast spliced aligner with low memory requirements. Nature Methods **12**: 357–360

Lisón P, Tárraga S, López-Gresa P, Saurí A, Torres C, Campos L, Bellés JM, Conejero V, Rodrigo I (2013) A noncoding plant pathogen provokes both transcriptional and posttranscriptional alterations in tomato. Proteomics **13**: 833–844

López-Dolz L, Spada M, Daròs J-A, Carbonell A (2020) Fine-tune control of targeted RNAi efficacy by plant artificial small RNAs. Nucleic Acids Research **48**: 6234–6250

Love MI, Huber W, Anders S (2014) Moderated estimation of fold change and dispersion for RNA-seq data with DESeq2. Genome Biology **15**: 550

Martin M (2011) Cutadapt removes adapter sequences from high-throughput sequencing reads. EMBnet.journal **17**: 10–12

Matousek J, Schroder AR, Trnena L, Reimers M, Baumstark T, Dedic P, Vlasak J, Becker I, Kreuzaler F, Fladung M, et al (1994) Inhibition of viroid infection by antisense RNA expression in transgenic plants. Biological chemistry Hoppe-Seyler **375**: 765–77

Minoia S, Carbonell A, Di Serio F, Gisel A, Carrington JC, Navarro B, Flores R (2014) Specific argonautes selectively bind small RNAs derived from potato spindle tuber viroid and attenuate viroid accumulation in vivo. Journal of Virology **88**: 11933–45

Mishra MK, Srivastava M, Singh G, Tiwari S, Niranjan A, Kumari N, Misra P (2017) Overexpression of Withania somnifera SGTL1 gene resists the interaction of fungus Alternaria brassicicola in Arabidopsis thaliana. Physiological and Molecular Plant Pathology **97**: 11–19

Mishra MK, Tiwari S, Misra P (2021) Overexpression of WssgtL3.1 gene from Withania somnifera confers salt stress tolerance in Arabidopsis. Plant Cell Reports. doi: 10.1007/s00299-021-02666-9

Montgomery TA, Howell MD, Cuperus JT, Li D, Hansen JE, Alexander AL, Chapman EJ, Fahlgren N, Allen E, Carrington JC (2008) Specificity of ARGONAUTE7-miR390 interaction and dual functionality in TAS3 trans-acting siRNA formation. Cell **133**: 128–41

Moreau RA, Whitaker BD, Hicks KB (2002) Phytosterols, phytostanols, and their conjugates in foods: structural diversity, quantitative analysis, and health-promoting uses. Progress in Lipid Research **41**: 457–500

Navarro B, Flores R, Di Serio F (2021a) Advances in Viroid-Host Interactions. Annual Review of Virology **8**: 305–325

Navarro B, Gisel A, Serra P, Chiumenti M, Di Serio F, Flores R (2021b) Degradome Analysis of Tomato and Nicotiana benthamiana Plants Infected with Potato Spindle Tuber Viroid. International Journal of Molecular Sciences **22**: 3725

Nelson D, Werck-Reichhart D (2011) A P450-centric view of plant evolution. The Plant Journal **66**: 194–211

Okamoto M, Kuwahara A, Seo M, Kushiro T, Asami T, Hirai N, Kamiya Y, Koshiba T, Nambara E (2006) CYP707A1 and CYP707A2, Which Encode Abscisic Acid 8′-Hydroxylases, Are Indispensable for Proper Control of Seed Dormancy and Germination in Arabidopsis. Plant Physiology **141**: 97–107

Owens RA, Gómez G, Lisón P, Conejero V (2017) Chapter 10 - Changes in the Host Proteome and Transcriptome Induced by Viroid Infection. *In* A Hadidi, R Flores, JW Randles, P Palukaitis, eds, Viroids and Satellites. Academic Press, Boston, pp 105–114

Pallás V, Gómez G (2017) Chapter 8 - Viroid Movement. *In* A Hadidi, R Flores, JW Randles, P Palukaitis, eds, Viroids and Satellites. Academic Press, Boston, pp 83–91

Pandey V, Niranjan A, Atri N, Chandrashekhar K, Mishra MK, Trivedi PK, Misra P (2014) WsSGTL1 gene from Withania somnifera, modulates glycosylation profile, antioxidant system and confers biotic and salt stress tolerance in transgenic tobacco. Planta **239**: 1217–1231

Pook VG, Nair M, Ryu K, Arpin JC, Schiefelbein J, Schrick K, DeBolt S (2017) Positioning of the SCRAMBLED receptor requires UDP-Glc:sterol glucosyltransferase 80B1 in Arabidopsis roots. Scientific Reports **7**: 5714

Ramirez-Estrada K, Castillo N, Lara JA, Arró M, Boronat A, Ferrer A, Altabella T (2017) Tomato UDP-Glucose Sterol Glycosyltransferases: A Family of Developmental and Stress Regulated Genes that Encode Cytosolic and Membrane-Associated Forms of the Enzyme. Frontiers in Plant Science. doi: 10.3389/fpls.2017.00984

Roche Y, Gerbeau-Pissot P, Buhot B, Thomas D, Bonneau L, Gresti J, Mongrand S, Perrier-Cornet J-M, Simon-Plas F (2008) Depletion of phytosterols from the plant plasma membrane provides evidence for disruption of lipid rafts. The FASEB Journal **22**: 3980–3991

Rodio ME, Delgado S, Flores R, Di Serio F (2006) Variants of Peach latent mosaic viroid inducing peach calico: uneven distribution in infected plants and requirements of the insertion containing the pathogenicity determinant. The Journal of general virology **87**: 231–40

Saema S, Rahman L ur, Singh R, Niranjan A, Ahmad IZ, Misra P (2016) Ectopic overexpression of WsSGTL1, a sterol glucosyltransferase gene in Withania somnifera, promotes growth, enhances glycowithanolide and provides tolerance to abiotic and biotic stresses. Plant Cell Rep **35**: 195–211

Sano T, Nagayama A, Ogawa T, Ishida I, Okada Y (1997) Transgenic potato expressing a double-stranded RNA-specific ribonuclease is resistant to potato spindle tuber viroid. Nature biotechnology **15**: 1290–4

Schwind N, Zwiebel M, Itaya A, Ding B, Wang MB, Krczal G, Wassenegger M (2009) RNAi-mediated resistance to Potato spindle tuber viroid in transgenic tomato expressing a viroid hairpin RNA construct. Molecular Plant Pathology **10**: 459–69

Semancik JS, Vanderwoude WJ (1976) Exocortis viroid: Cytopathic effects at the plasma membrane in association with pathogenic RNA. Virology **69**: 719–726

Sharma M, Sasvari Z, Nagy PD (2010) Inhibition of sterol biosynthesis reduces tombusvirus replication in yeast and plants. Journal of Virology **84**: 2270–81

Singh G, Tiwari M, Singh SP, Singh S, Trivedi PK, Misra P (2016) Silencing of sterol glycosyltransferases modulates the withanolide biosynthesis and leads to compromised basal immunity of Withania somnifera. Scientific Reports **6**: 1–13

Takeuchi J, Fukui K, Seto Y, Takaoka Y, Okamoto M (2021) Ligand–receptor interactions in plant hormone signaling. The Plant Journal **105**: 290–306

Tsuda S, Sano T (2014) Threats to Japanese agriculture from newly emerged plant viruses and viroids. Journal of General Plant Pathology **80**: 2–14

Vázquez Prol F, López-Gresa MP, Rodrigo I, Bellés JM, Lisón P (2020) Ethylene is Involved in Symptom Development and Ribosomal Stress of Tomato Plants upon Citrus Exocortis Viroid Infection. Plants **9**: 582

Vázquez Prol F, Márquez-Molins J, Rodrigo I, López-Gresa MP, Bellés JM, Gómez G, Pallás V, Lisón P (2021) Symptom Severity, Infection Progression and Plant Responses in Solanum Plants Caused by Three Pospiviroids Vary with the Inoculation Procedure. International Journal of Molecular Sciences **22**: 6189

Wickham H (2016). ggplot2: Elegant Graphics for Data Analysis. Springer-Verlag New York. ISBN 978-3-319-24277-4.

Yang X, Yie Y, Zhu F, Liu Y, Kang L, Wang X, Tien P (1997) Ribozyme-mediated high resistance against potato spindle tuber viroid in transgenic potatoes. Proceedings of the National Academy of Sciences of the United States of America **94**: 4861–5

Zhu JY, Sae-Seaw J, Wang ZY (2013) Brassinosteroid signalling. Development **140**: 1615–20

FIGURE CAPTIONS

Figure 1. *Solanum lycopersicum* cv. Moneymaker T1 transgenic lines expressing amiR-PSTVd, an artificial microRNA (amiRNA) against *Potato spindle tuber viroid* (PSTVd). **A**, Diagram of the anti-PSTVd amiRNA construct, *35S:amiR-PSTVd*, engineered to express amiR-PSTVd from *Arabidopsis thaliana MIR390a* (*AtMIR390a*) precursor (in black). amiRNA and star strand positions in *AtMIR390a* are indicated with light and dark blue, respectively. Coordinates of the complete target site in PSTVd are given. The arrow indicates the amiRNA-predicted cleavage site. **B**, Photographs taken at 10 days post transplanting of representative tomato lines expressing anti-PSTVd amiRNA and of a non-transgenic control (NTC) plant. **C**, Northern blot detection of amiR-PSTVd in RNA preparations from apical leaves of tomato plants. The U6 blot is shown as the loading control.

Figure 2. Functional analysis of the anti-*Potato spindle tuber viroid* (PSTVd) artificial microRNA (amiRNA) construct in transgenic *Solanum lycopersicum* plants. **A**, Two-dimensional line graph show, for each three-plant set listed in the box, the percentage of symptomatic plants per day for 20 days post-inoculation (dpi). **B**, Photographs taken at four weeks post-inoculation (wpi) of representative transgenic tomato plants expressing amiR-PSTVd and of non-transgenic control (NTC) plants. **C**, Accumulation of PSTVd, and of *SlPR1* and *SlNAC082* mRNAs in tomato plants. Bar graphs show mean relative level + standard error of PSTVd (pink), and of *SlPR1* (green) and *SlNAC082* (orange) mRNAs at 2 wpi (left) and at 4 wpi (right) after normalization to *ACTIN* (*SlACT*) and *EXPRESSED PROTEIN* (*SlEXP*), as determined by quantitative RT-PCR (RT-qPCR) (NTC + PSTVd = 1 in all comparisons). For each target, bars with an asterisc are statistically significantly different from that of samples NTC + PSTVd (P<0.05 in pair-wise Student's t-test comparisons).

Figure 3. Phenotypic analysis of adult *Solanum lycopersicum* transgenic lines expressing an artificial microRNA (amiRNA) against *Potato spindle tuber viroid* (PSTVd). **A**, Photographs taken at eight weeks post transplanting (wpt) of representative tomato T1 plants expressing

anti-PSTVd amiRNA and of a non-transgenic control (NTC) plant. **B**, Phenotypic analysis at 8 wpt of adult plants including NTC plants and amiRNA transgenic lines. Top, bar graphs show mean + standard deviation of plant height (cm). Bottom, bar graph shows mean + standard deviation of internode length (cm). Bars with an asterisc are statistically significantly different from that of NTC samples ($P<0.05$ in pair-wise Student's t-test comparisons). **C**, Photographs of representative tomato fruits from a NTC and two amiRNA lines. **D**, Phenotypic analysis of tomato fruits from NTC and amiRNA lines. Left, mean + standard deviation of fresh weight. Right, mean + standard deviation of diameter. Other details are as in B.

Figure 4. Molecular analysis of adult *Solanum lycopersicum* transgenic lines expressing an artificial microRNA (amiRNA) against *Potato spindle tuber viroid* (PSTVd). **A**, MA plot shows log2 fold change versus mean expression of genes in four amiRNA lines (1, 2, 5 and 16) compared with four non-transgenic control (NTC) lines. Green, red and grey dots represent differentially underexpressed, differentially overexpressed or non-differentially expressed genes, respectively, in amiRNA versus control comparison. **B**, Accumulation of *SlSGT1* mRNA in tomato plants. Bar graphs show mean relative level + standard error of *SlSGT1* mRNAs at eight weeks post transplanting (wpi) after normalization to *ACTIN* (*SlACT*) and *EXPRESSED PROTEIN* (*SlEXP*), as determined by quantitative RT-PCR (RT-qPCR) (NTC-1 = 1 in all comparisons). Other details are as in Figure 2C. **C**, 5' RLM-RACE analysis of amiR-PSTVd-guided cleavage of *SlSGT1*. At the top panel, the predicted base-pairing between amiR-PSTVd and *SlSGT1* mRNA is shown, and the expected amiR-PSTVd-based cleavage site is indicated by an arrow. The proportion of cloned 5'-RLM-RACE products at the at the expected cleavage site is shown for amiR-PSTVd-expressing lines. TPS refers to "Target Prediction Score". At the bottom panel, ethidium bromide-stained gel shows 5'-RLM-RACE products corresponding to the 3' cleavage product from amiR-PSTVd-guided cleavage (top gel), and RT-PCR products corresponding to the control *SlACT* gene (bottom gel). The position and size of the expected amiRNA-based 5'-RLM-RACE products are indicated, as well as the position and size of control RT-PCR products. **D**, Sterol analysis. Bar graph shows the mean relative content + standard deviation of sterol glycosides (dark purple) and free sterols (light purple) in NTC and amiRNA lines at 8 wpt. Other details are as in Figure 2C.

Figure 5. Analysis of putative down-regulation of *SlSGT1* mRNA in non-transgenic *Solanum lycopersicum* control plants (NTCs) during *Potato spindle tuber viroid* infection. **A**, Sequence alignment between amiR-PSTVd and three PSTVd sRNAs of (-) polarity highly enriched in AGO1 immunoprecipitations. The sequence shared by each PSTVd sRNA with amiR-PSTVd is highlighted in a square. **B**, 5' RLM-RACE analysis of putative PSTVd sRNA-guided cleavage of *SlSGT1*. At the top panel, the predicted base-pairing between a PSTVd (-) sRNA and *SlSGT1* mRNA is shown, and the expected cleavage site is indicated by an arrow. Other details are as in Figure 4C. **C**, Bar graph shows mean relative level + standard error of *SlSGT1* mRNAs at two and four weeks post inoculation (wpi) after normalization to *ACTIN* (*SlACT*) and *EXPRESSED PROTEIN* (*SlEXP*), as determined by quantitative RT-PCR (RT-qPCR) (NTC 2 wpi = 1 in all comparisons). Other details are as in Figure 2C. At the bottom panel, ethidium bromide-stained gel shows 5'-RLM-RACE products corresponding to the 3' cleavage product from amiR-PSTVd-guided cleavage (top gel). ns refers to non-statistically significant in the corresponding pair-wise Students's t-test comparison. Other details are as in Figure 2C and 4C.

Figure 6. Functional analysis of *Solanum lycopersicum* cv. Micro-Tom transgenic lines expressing amiRNAs against *STEROL GLYCOSILTRANSFERASE1* (*SlSGT1*). **A**, Diagram of the two anti-SlSGT1 amiRNA constructs, *35S:amiR-SlSGT1-1 and 35S:amiR-SlSGT1-2*, engineered to express amiRNAs from *Arabidopsis thaliana MIR319a* (*AtMIR319a*) precursor (in black). amiRNA and star strand positions in *AtMIR319a* are indicated with brown and dark blue, respectively. Coordinates of the complete target site in *SlSGT1* mRNA are given. Other details are as in Figure 1A. **B**, Two-dimensional line graph show, for each three-plant set listed in the box, the percentage of symptomatic plants per day for 20 days post-inoculation (dpi). **C**, Photographs taken at two weeks post inoculation (wpi) of representative transgenic tomato plants expressing amiR-PSTVd and of non-transgenic control (NTC) plants. **D**, Accumulation of PSTVd, and of *SlPR1*, *SlNAC082* and *SlSGT1* mRNAs in tomato plants. Bar graphs show mean relative level + standard error of PSTVd (pink), and of *SlPR1* (green), *SlNAC082* (orange) and *SlSGT1* (purple) mRNAs at 2 wpi (left) and at 4 wpi (right) after

normalization to *ACTIN* (*SlACT*) and *EXPRESSED PROTEIN* (*SlEXP*), as determined by quantitative RT-PCR (RT-qPCR) (NTC + PSTVd = 1 in all comparisons). Other details are as in Figure 2C.

Figure 7. Model establishing the relationship between *SlSGT1*, *SlNAC082* and *SlPR1* expression and PSTVd-induced symptomatology.

Table 1. Top putative amiR-PSTVd off-targets identified from target prediction analysis.

Putative off-target	Description	TPS[a]	Log2 fold change	p-adj	DE[b]
Solyc02g037540.3	Disease resistance protein	4.5	-	-	-
Solyc11g072610.3	DNA repair (Rad51) family protein	5	-	-	-
Solyc06g007980.4	Sterol 3-beta-glycosyltransferase 1	5.5	-3.2536	$3.32x10^{-22}$	Yes
Solyc05g025900.3	MT.1	5.5	-0.0092	0.9965	No
Solyc11g005700.1	RING-type E3 ubiquitin transferase	5.5	0.5618	0.1409	No
Solyc02g084620.3	Forkhead-associated (FHA) domain	6	-0.1747	0.7942	No
Solyc05g053670.3	60S ribosomal protein L13a	6	-0.1791	0.7614	No
Solyc08g065940.5	Zinc finger CCCH domain-containing protein 20	6	-	-	-
Solyc10g078480.2	Chitobiosyldiphosphodolichol beta-mannosyltransferase-like protein	6	-0.0367	0.9889	No
Solyc12g009400.2	Pyruvate dehydrogenase	6	-0.0517	0.9464	No
Solyc12g009410.2	Pyruvate dehydrogenase	6	-0.1918	0.5941	No
Solyc01g103010.4	Cullin-associated NEDD8-dissociated protein.1	6	-0.0384	0.9702	No

[a]TPS refers to target prediction score used by P-SAMS (Fahlgren et al. 2016)

[b]DE refers to differentially expressed, with a falsed discovery rate of 1%

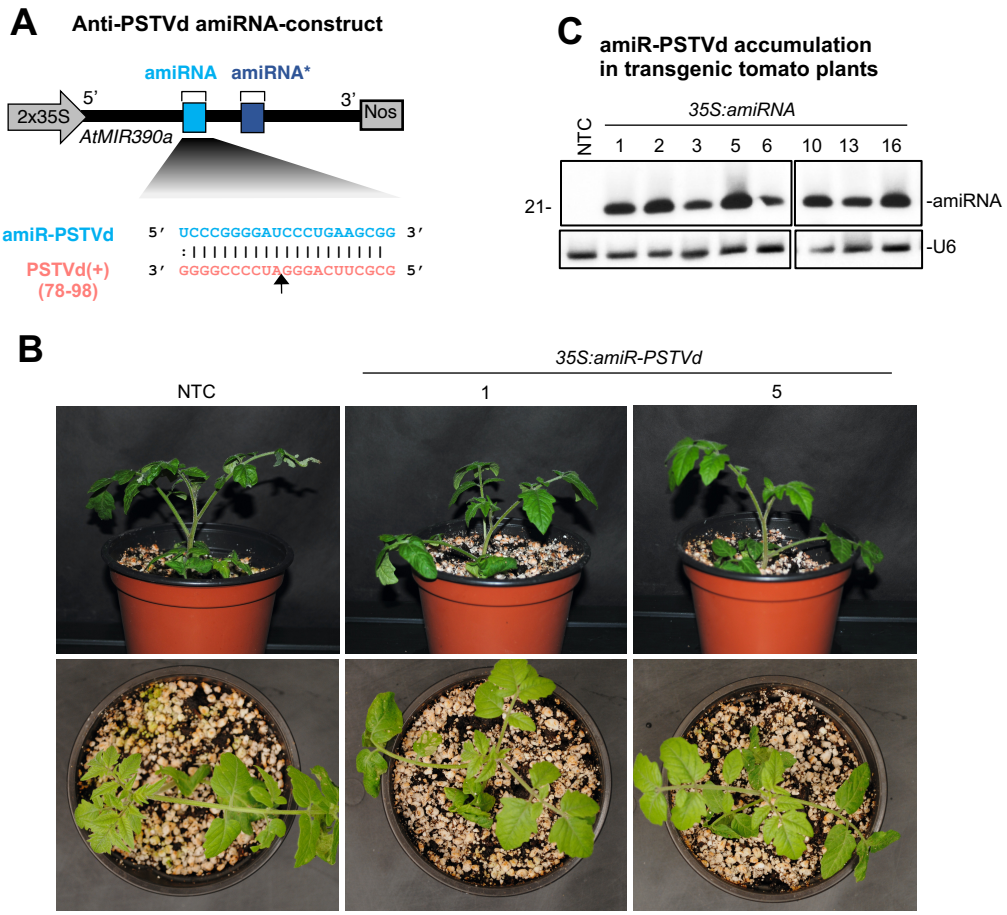

Figure 1. *Solanum lycopersicum* cv. Moneymaker T1 transgenic lines expressing amiR-PSTVd, an artificial microRNA (amiRNA) against *Potato spindle tuber viroid* (PSTVd). **A**, Diagram of the anti-PSTVd amiRNA construct, *35S:amiR-PSTVd*, engineered to express amiR-PSTVd from *Arabidopsis thaliana MIR390a* (*AtMIR390a*) precursor (in black). amiRNA and star strand positions in *AtMIR390a* are indicated with light and dark blue, respectively. Coordinates of the complete target site in PSTVd are given. The arrow indicates the amiRNA-predicted cleavage site. **B**, Photographs taken at 10 days post transplanting of representative tomato lines expressing anti-PSTVd amiRNA and of a non-transgenic control (NTC) plant. **C**, Northern blot detection of amiR-PSTVd in RNA preparations from apical leaves of tomato plants. The U6 blot is shown as the loading control.

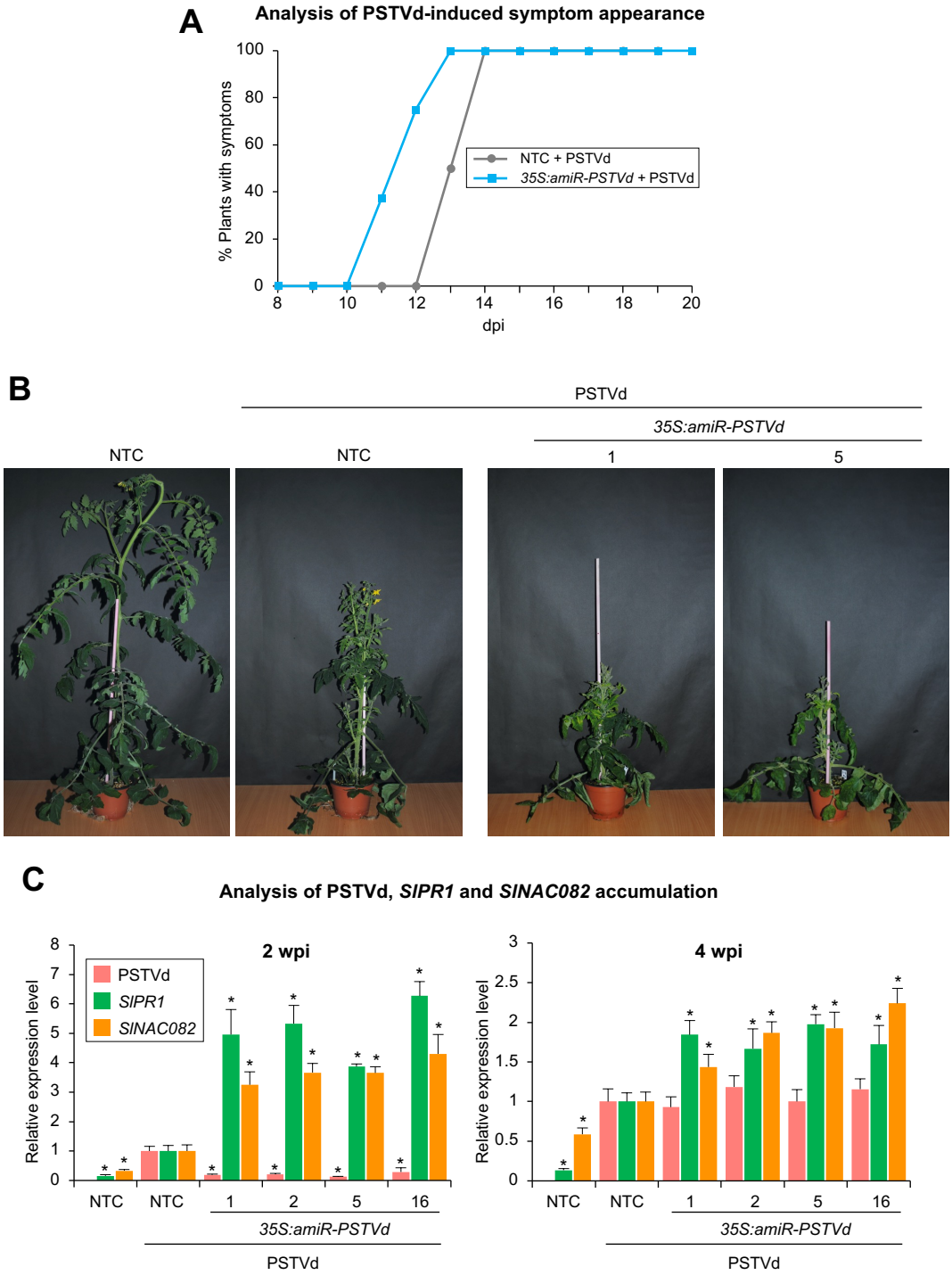

Figure 2. Functional analysis of the anti-*Potato spindle tuber viroid* (PSTVd) artificial microRNA (amiRNA) construct in transgenic *Solanum lycopersicum* plants. **A**, Two-dimensional line graph show, for each three-plant set listed in the box, the percentage of symptomatic plants per day for 20 days post-inoculation (dpi). **B**, Photographs taken at four weeks post-inoculation (wpi) of representative transgenic tomato plants expressing amiR-PSTVd and of non-transgenic control (NTC) plants. **C**, Accumulation of PSTVd, and of *SlPR1* and *SlNAC082* mRNAs in tomato plants. Bar graphs show mean relative level + standard error of PSTVd (pink), and of *SlPR1* (green) and *SlNAC082* (orange) mRNAs at 2 wpi (left) and at 4 wpi (right) after normalization to *ACTIN* (*SlACT*) and *EXPRESSED PROTEIN* (*SlEXP*), as determined by quantitative RT-PCR (RT-qPCR) (NTC + PSTVd = 1 in all comparisons). For each target, bars with an asterisc are statistically significantly different from that of samples NTC + PSTVd ($P<0.05$ in pair-wise Student's t-test comparisons).

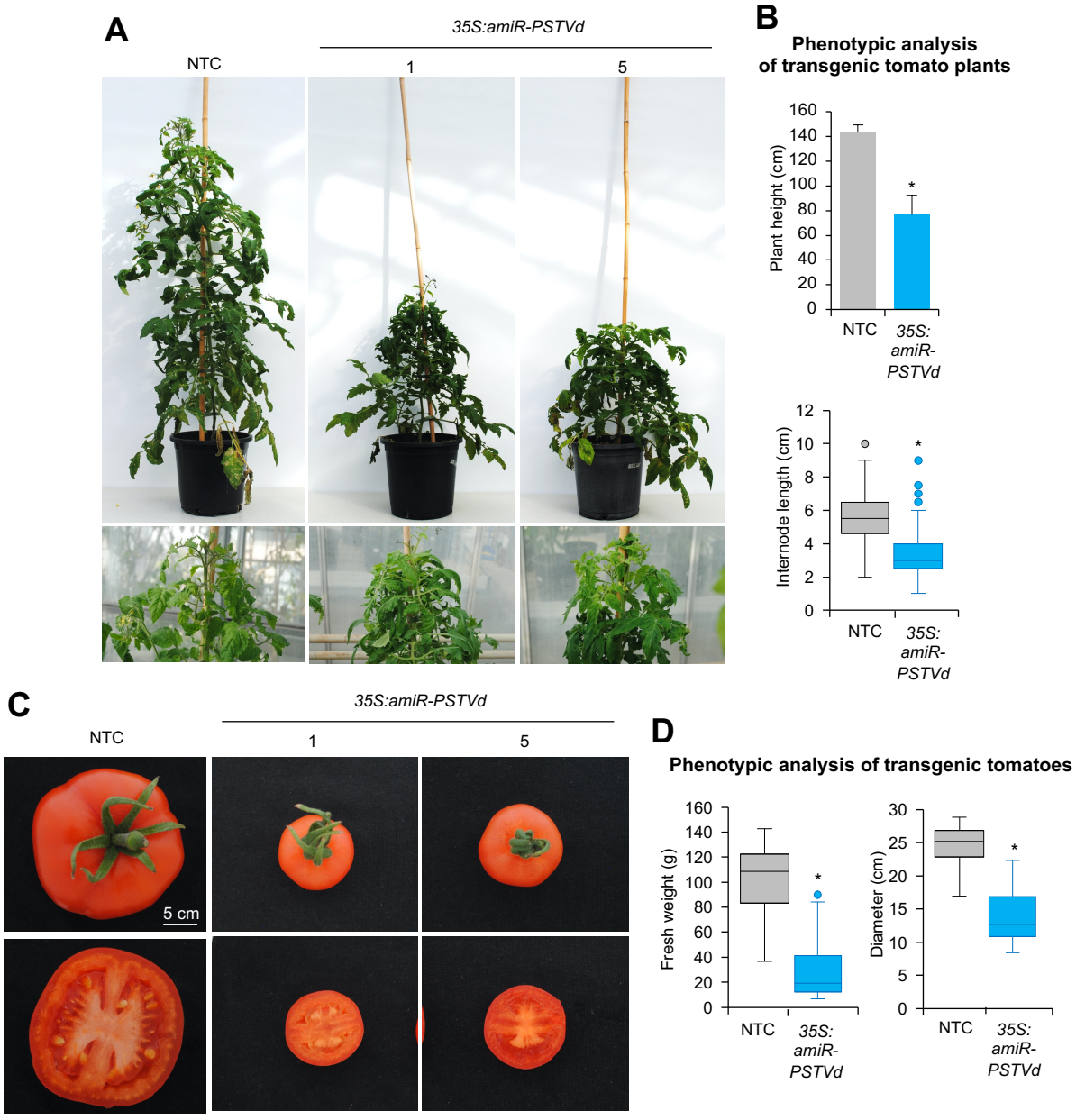

Figure 3. Phenotypic analysis of adult *Solanum lycopersicum* transgenic lines expressing an artificial microRNA (amiRNA) against *Potato spindle tuber viroid* (PSTVd). **A**, Photographs taken at eight weeks post transplanting (wpt) of representative tomato T1 plants expressing anti-PSTVd amiRNA and of a non-transgenic control (NTC) plant. **B**, Phenotypic analysis at 8 wpt of adult plants including NTC plants and amiRNA transgenic lines. Top, bar graphs show mean + standard deviation of plant height (cm). Bottom, bar graph shows mean + standard deviation of internode length (cm). Bars with an asterisc are statistically significantly different from that of NTC samples ($P<0.05$ in pair-wise Student's t-test comparisons). **C**, Photographs of representative tomato fruits from a NTC and two amiRNA lines. **D**, Phenotypic analysis of tomato fruits from NTC and amiRNA lines. Left, mean + standard deviation of fresh weight. Right, mean + standard deviation of diameter. Other details are as in B.

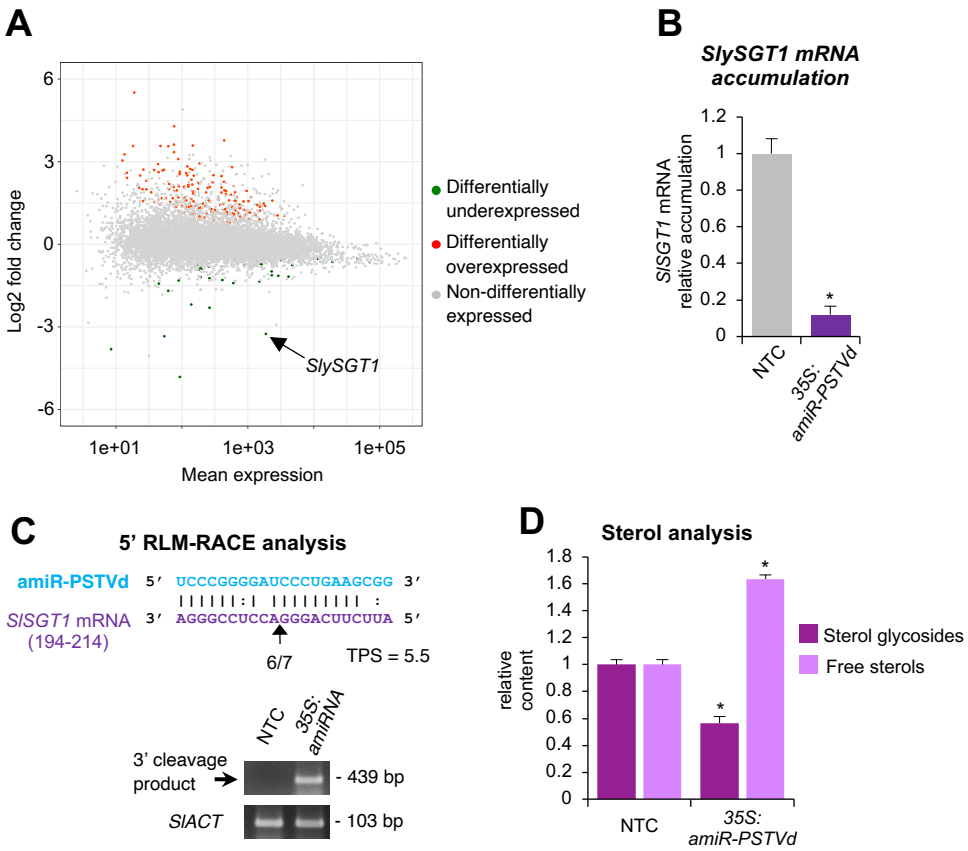

Figure 4. Molecular analysis of adult *Solanum lycopersicum* transgenic lines expressing an artificial microRNA (amiRNA) against *Potato spindle tuber viroid* (PSTVd). **A**, MA plot shows log2 fold change versus mean expression of genes in four amiRNA lines (1, 2, 5 and 16) compared with four non-transgenic control (NTC) lines. Green, red and grey dots represent differentially underexpressed, differentially overexpressed or non-differentially expressed genes, respectively, in amiRNA versus control comparison. **B**, Accumulation of *SlSGT1* mRNA in tomato plants. Bar graphs show mean relative level + standard error of *SlSGT1* mRNAs at eight weeks post transplanting (wpi) after normalization to *ACTIN* (*SlACT*) and *EXPRESSED PROTEIN* (*SlEXP*), as determined by quantitative RT-PCR (RT-qPCR) (NTC-1 = 1 in all comparisons). Other details are as in Figure 2C. **C**, 5' RLM-RACE analysis of amiR-PSTVd-guided cleavage of *SlSGT1*. At the top panel, the predicted base-pairing between amiR-PSTVd and *SlSGT1* mRNA is shown, and the expected amiR-PSTVd-based cleavage site is indicated by an arrow. The proportion of cloned 5'-RLM-RACE products at the at the expected cleavage site is shown for amiR-PSTVd-expressing lines. TPS refers to "Target Prediction Score". At the bottom panel, ethidium bromide-stained gel shows 5'-RLM-RACE products corresponding to the 3' cleavage product from amiR-PSTVd-guided cleavage (top gel), and RT-PCR products corresponding to the control *SlyACT* gene (bottom gel). The position and size of the expected amiRNA-based 5'-RLM-RACE products are indicated, as well as the position and size of control RT-PCR products. **D**, Sterol analysis. Bar graph show the mean relative content + standard deviation of sterol glycosides (dark purple) and free sterols (light purple) in NTC and amiRNA lines at 8 wpt. Other details are as in Figure 2C.

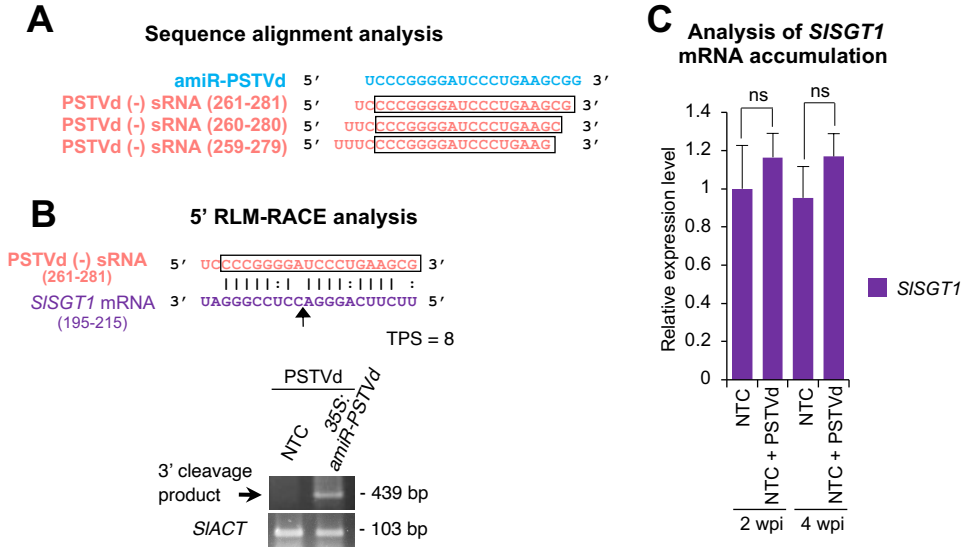

Figure 5. Analysis of putative down-regulation of *SlSGT1* mRNA in non-transgenic *Solanum lycopersicum* control plants (NTCs) during *Potato spindle tuber viroid* infection. **A**, Sequence alignment between amiR-PSTVd and three PSTVd sRNAs of (-) polarity highly enriched in AGO1 immunoprecipitations. The sequence shared by each PSTVd sRNA with amiR-PSTVd is highlighted in a square. **B**, 5' RLM-RACE analysis of putative PSTVd sRNA-guided cleavage of *SlSGT1*. At the top panel, the predicted base-pairing between a PSTVd (-) sRNA and *SlSGT1* mRNA is shown, and the expected cleavage site is indicated by an arrow. Other details are as in Figure 4C. **C**, Bar graph shows mean relative level + standard error of *SlSGT1* mRNAs at two and four weeks post inoculation (wpi) after normalization to *ACTIN* (*SlACT*) and *EXPRESSED PROTEIN* (*SlEXP*), as determined by quantitative RT-PCR (RT-qPCR) (NTC 2 wpi = 1 in all comparisons). Other details are as in Figure 2C. At the bottom panel, ethidium bromide-stained gel shows 5'-RLM-RACE products corresponding to the 3' cleavage product from amiR-PSTVd-guided cleavage (top gel). ns refers to non-statistically significant in the corresponding pair-wise Students's t-test comparison. Other details are as in Figure 2C and 4C.

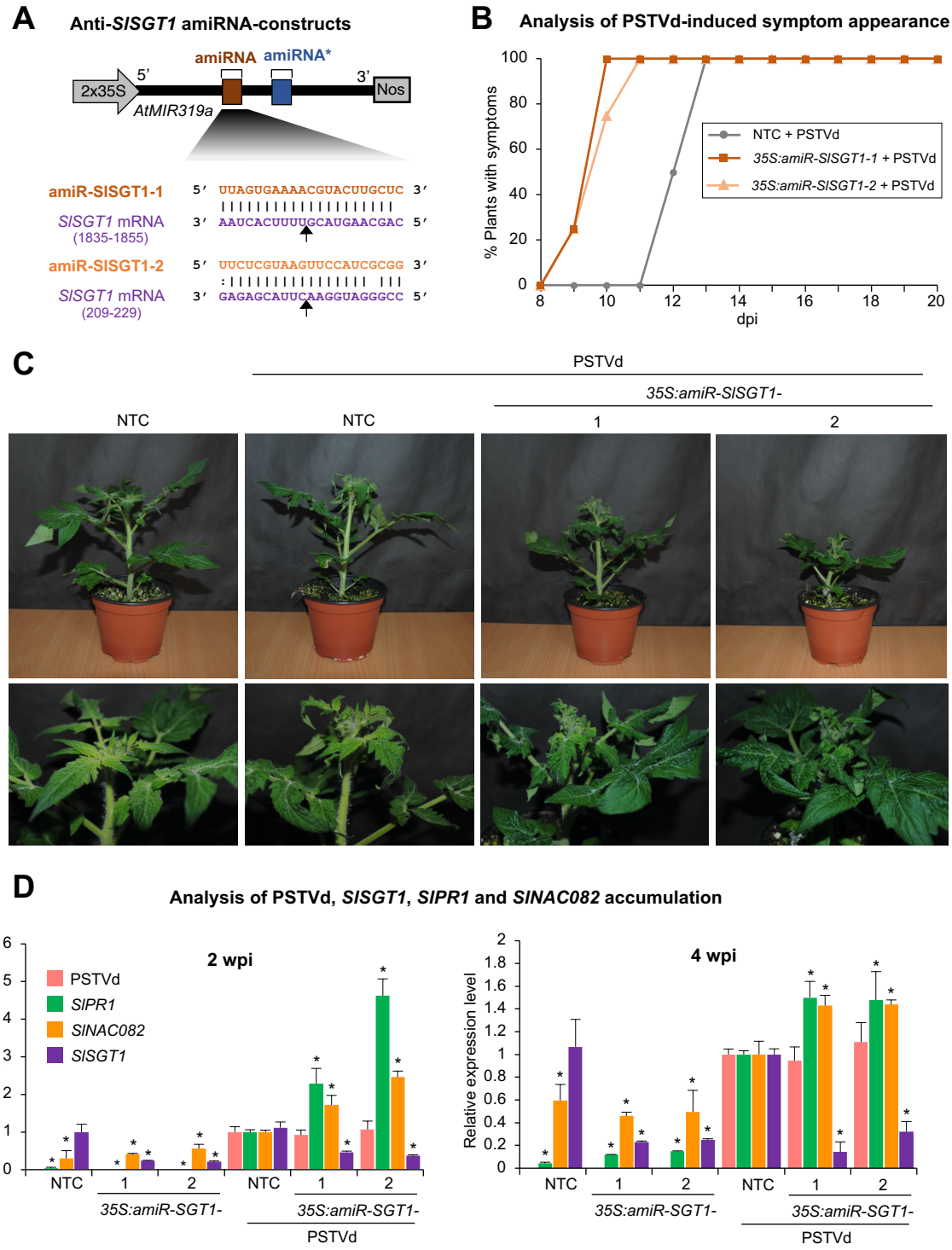

Figure 6. Functional analysis of *Solanum lycopersicum* cv. Micro-Tom transgenic lines expressing amiRNAs against *STEROL GLYCOSILTRANSFERASE1* (*SlSGT1*). **A**, Diagram of the two anti-SlSGT1 amiRNA constructs, *35S:amiR-SlSGT1-1 and 35S:amiR-SlSGT1-2*, engineered to express amiRNAs from *Arabidopsis thaliana MIR319a* (*AtMIR319a*) precursor (in black). amiRNA and star strand positions in *AtMIR319a* are indicated with brown and dark blue, respectively. Coordinates of the complete target site in *SlSGT1* mRNA are given. Other details are as in Figure 1A. **B**, Two-dimensional line graph show, for each three-plant set listed in the box, the percentage of symptomatic plants per day for 20 days post-inoculation (dpi). **C**, Photographs taken at two weeks post inoculation (wpi) of representative transgenic tomato plants expressing amiR-PSTVd and of non-transgenic control (NTC) plants. **D**, Accumulation of PSTVd, and of *SlPR1*, *SlNAC082* and *SlSGT1* mRNAs in tomato plants. Bar graphs show mean relative level + standard error of PSTVd (pink), and of *SlPR1* (green), *SlNAC082* (orange) and *SlSGT1* (purple) mRNAs at 2 wpi (left) and at 4 wpi (right) after normalization to *ACTIN* (*SlACT*) and *EXPRESSED PROTEIN* (*SlEXP*), as determined by quantitative RT-PCR (RT-qPCR) (NTC + PSTVd = 1 in all comparisons). Other details are as in Figure 2C.

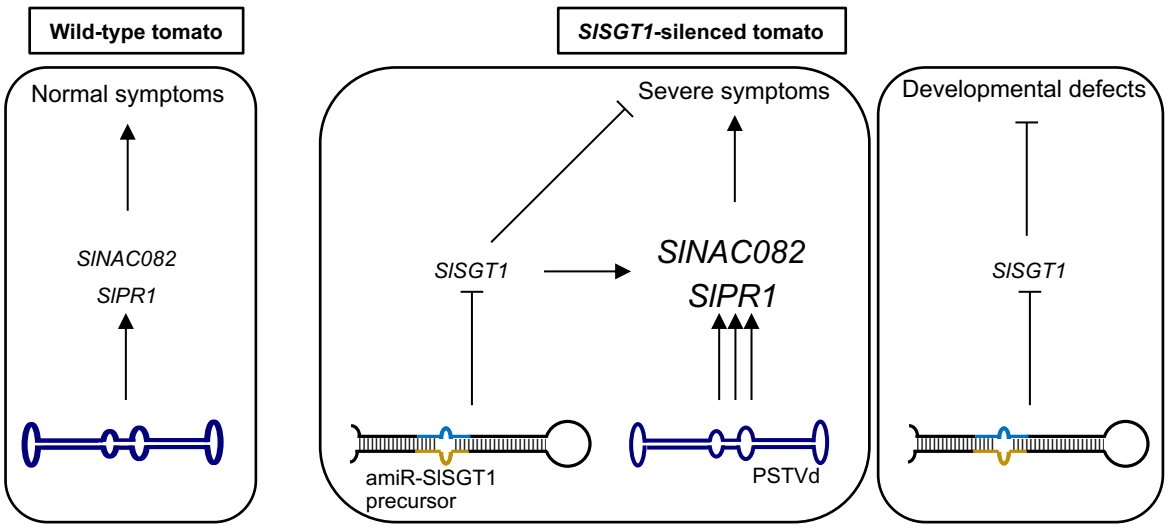

Figure 7. Model establishing the relationship between *SlSGT1*, *SlNAC082* and *SlPR1* expression and PSTVd-induced symptomatology.